Robust H_∞ Control Implementation in IFOC for High-Performance Electric Vehicle Induction Motors

Abdelhak Boudallaa [1,2]*, *Mohammed* Chennani[1], *Ahmed* Belkhadir [1, 3], *Karim* Rhofir [2] and *Driss* Belkhayat[1]
[1] Univ. Cadi Ayyad, P.O. Box 549, Laboratoire des Systèmes Electriques, Efficacité Energétique et Télécommunications (LSEEET), Marrakesh, Morocco.
[2] Laboratoire des Sciences et Techniques pour l'Ingénieur (LaSTI)
Ecole nationale des sciences appliquées (ENSAK), Khouribga, Morocco
[3] Univ. Artois, UR 4025, Laboratoire Systèmes Electrotechniques et Environnement (LSEE), F-62400 Béthune, France.

Abstract. This paper presents an indirect field-oriented control method with rotor flux orientation applied to induction motors, enhanced by robust controllers. This approach aims to optimize the motor's dynamic performance, allowing for more precise control of torque and speed. Due to the nonlinear, multivariable, and highly coupled dynamics, induction motors require particularly complex control algorithms. Consequently, this method relies on accurate knowledge of the rotor position, which is directly related to the rotor time constant and, under real conditions, depends on temperature variations as well as the magnetic state of the machine. This technique was simulated in MATLAB/Simulink environment and subsequently implemented in real time.

Keywords. Electrical vehicle, induction Motor, field-oriented control, $\boldsymbol{H}_\infty$ controller, dSpace 1104

1 Symbol and Nomenclature

- IFOC: Indirect Flux Oriented Control;
- FCS: Fuel Cell System;
- SES: Secondary Energy System;
- $\mathrm{R_s}$, $\mathrm{R_r}$: Stator and rotor resistances of the motor;
- $\mathrm{L_s}$, $\mathrm{L_r}$ et $\mathrm{L_m}$: Stator, rotor, and mutual inductances;
- i_{dq}: Stator currents;
- v_{dq}: Stator voltages;
- p: Number of pole pairs.

2 Introduction

The main challenge in controlling an Induction Machine (IM) is that torque and flux are highly coupled variables, meaning that any action on one directly affects the other. In contrast, in a separately excited DC machine, these two variables are naturally decoupled, which explains the simplicity of controlling such machines.
Recent advances in power and digital electronics have made the efficient control of variable-speed drives for IM feasible-capabilities that were once limited to DC motors. However, due to nonlinear, multivariable, highly coupled, and uncertain dynamics, IMs require increasingly complex control algorithms as higher performance is demanded. To address these challenges, various control strategies have been developed to manage the real-time control of flux and electromagnetic torque in IMs. The most prominent strategy is vector control through flux orientation [1]. This approach aims to replicate, from the user's perspective, the performance of a separately excited DC motor when applied to an IM. The technique relies on the use of IP controllers for speed and PI controllers for the direct and quadrature currents of the motor [2].
Enhancing the IFOC strategy with H_∞ technique is used to improve the performance of IM. The H_∞ technique is used for the rapid development of robust control laws for stationary and multivariable linear systems and is gaining increasing importance among controller design methods. A key advantage of this approach is its ability to explicitly consider frequency and time-domain specifications from the design requirements, which are directly translated into a mathematical criterion that

* Corresponding author: boudallaa.abdelhak@gmail.com

must be satisfied. The controller design meeting this criterion is algorithmically achieved by solving an optimization problem, utilizing the computational power of modern computers [3, 4].
For the synthesis of a H_∞ control law, it is essential to use a relatively simple model of the process. This approach has the advantage of yielding a low-order controller, which simplifies both analysis and implementation. However, to ensure that the performance predicted by the synthesis model is achieved on the real system, a robustness analysis must be conducted [5].
This paper is organized as follows: the first section provides a description of the traction chain and the dynamic modelling of IM, followed by an explanation of the IFOC principle with rotor flux. The second section discusses the robust synthesis of controllers. Simulations of the IFOC strategy with PI controllers, as well as the IFOC strategy enhanced by robust controllers, conducted in MATLAB/Simulink are presented.
Finally, the implementation of the IFOC strategy in various vehicle driving scenarios is proposed [6].
The drive chain of the Electric Vehicle (EV) (Fig. 1) consists of three main electrical power components: the electric machine, the secondary energy source, and the fuel cell system. These elements are connected to one or more buses.

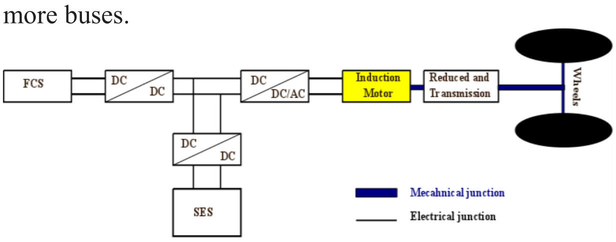

Fig. 1. Drive chain of an electric.

Reducing the energy consumption of EVs depends on several factors related to both design and vehicle usage. Key elements include optimized design, efficient energy management of various components, speed optimization, route planning, and the integration of advanced technologies. By combining these strategies, it is possible to significantly reduce energy consumption while improving the range and overall efficiency of EVs.
In the following section, the electric motor is considered the primary element responsible for energy consumption in the propulsion chain. Therefore, robust motor control can significantly improve the dynamic performances of IMs

3 Robust Modelling of Induction Motors

3.1 Modelling of Induction Motors

The dynamic model of the IM is expressed in the following form [7, 8]:

$$v_{sd} = \sigma L_s \frac{d}{dt} i_{sd} + \left(R_s + R_r \frac{L_m^2}{L_r^2}\right) i_{sd} - \sigma L_s \omega_s i_{sq} - R_r \frac{L_m}{L_r^2} \varphi_r \quad (1)$$

$$v_{sq} = \sigma L_s \frac{d}{dt} i_{sq} + \left(R_s + R_r \frac{L_m^2}{L_r^2}\right) i_{sq} + \sigma L_s \omega_s i_{sd} + \frac{L_m}{L_r} p\Omega\varphi_r \quad (2)$$

$$\left(1 + \frac{L_r}{R_r} \frac{d}{dt}\right) \varphi_r = L_m i_{sd} \quad (3)$$

$$\omega_s = (\omega_r + p\Omega)\ ; \omega_r = \frac{L_m R_r}{L_r \varphi_r} i_{sq} \quad (4)$$

$$T_{em} = p \frac{L_m}{L_r} \varphi_r\, i_{sq} \quad (5)$$

3.2 Input-output decoupling through compensation

In equations (1) and (2), we notice the existence of coupling between the d and q axes. The supply voltages v_{sd} and v_{sq} affect both i_{sd} and i_{sq}, and thus influence both the flux and the electromagnetic torque.

$$v_{sd} = \left(\sigma L_s s + \left(R_s + R_r \frac{L_m^2}{L_r^2}\right)\right) i_{sd} - e_{sq} \quad (6)$$

$$v_{sq} = \left(\sigma L_s s + \left(R_s + R_r \frac{L_m^2}{L_r^2}\right)\right) i_{sq} - e_{sd} \quad (7)$$

with:

$$e_{sd} = -\left(\sigma L_s \omega_s i_{sd} + \frac{L_m}{L_r} p\Omega\varphi_r\right) \quad (8)$$

$$e_{sq} = \sigma L_s \omega_s i_{sq} + R_r \frac{L_m}{L_r^2} \varphi_r \quad (9)$$

$$R_{sr} = R_s + R_r \frac{L_m^2}{L_r^2} \quad (10)$$

The voltage equations, with the two new control variables v_{sd1} and v_{sq1}, become:

$$v_{sd1} = (R_{sr} + \sigma L_s s) i_{sd} \quad (11)$$

$$v_{sq1} = (R_{sr} + \sigma L_s s) i_{sq} \quad (12)$$

Equations (11) and (12) allow for the synthesis of PI controllers for the currents i_{sd} and i_{sq}, while the speed controller used is of the IP type.
The block diagram of the speed control system for the IM using the proposed approach is illustrated in Fig. 2. The reference values are marked with the asterisk (*). For IM speeds below its nominal speed, the reference flux is typically kept constant [9, 10].

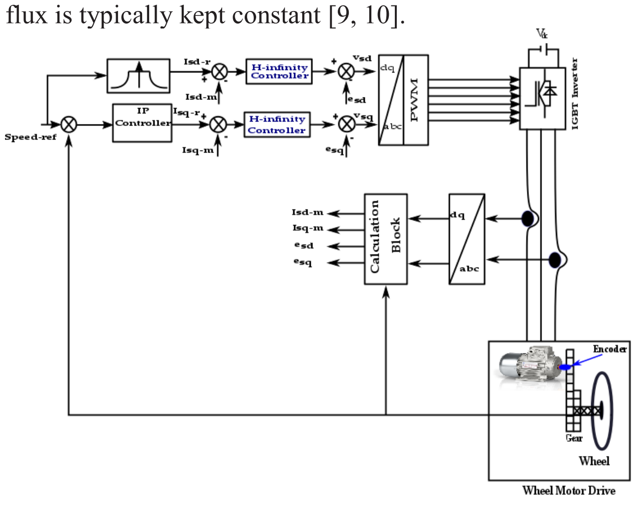

Fig. 2. Schematic diagram of the IFOC strategy.

4 Standard H_∞ synthesis

Consider the typical diagram of a closed-loop system configuration represented in Fig. 3, where G(s) represents the model of the system to be controlled and K(s) is the controller, whose role is to generate the commands to be applied based on the observed outputs and reference signals.

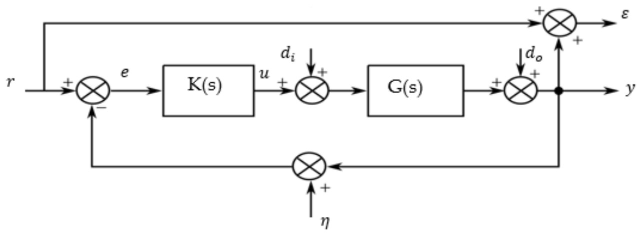

Fig. 3. Block diagram of a controlled system.

They are denoted, respectively, as S, T, SKS, and SGS. The first two are called, respectively, the sensitivity function and the complementary sensitivity function, as they represent the sensitivity of the system's quantities to external disturbance signals.

$$\begin{cases} T_{r\varepsilon} = [1 + K(s)G(s)]^{-1} \\ T_{ry} = K(s)G(s)[1 + K(s)G(s)]^{-1} \\ T_{ru} = K(s)[1 + K(s)G(s)]^{-1} \\ T_{d_i y} = G(s)[1 + K(s)G(s)]^{-1} \end{cases} \quad (13)$$

In the diagram of Fig. 4, by applying the weighting filters $W_e(s)$, $W_s(s)$ and $W_d(s)$ to the outputs $\tilde{e}$ and $\tilde{u}$ and to the input $\widetilde{d_i}$, respectively, we obtain two new signals to be controlled

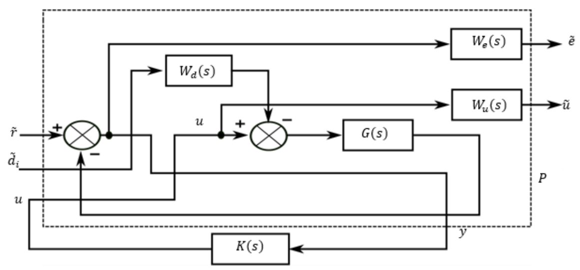

Fig. 4. Standard form of the synthesis diagram.

Referring to the problem represented by the diagram above, we can calculate the transfer matrix of the interconnected system. Thus, we obtain the equation:

$$\begin{bmatrix} \tilde{e} \\ \tilde{u} \end{bmatrix} = \begin{bmatrix} w_e(1 + KG)^{-1} & w_e G(1 + KG)^{-1} w_d \\ w_u K(1 + KG)^{-1} & w_u KG(1 + KG)^{-1} w_d \end{bmatrix} \begin{bmatrix} \tilde{r} \\ \widetilde{d_i} \end{bmatrix} \quad (14)$$

The standard H_∞ problem to be solved consists of finding a γ gammaγ and a transfer function K(s) that internally stabilizes the closed-loop system and satisfies the constraint

According to criterion (14) and the properties of the H_∞ norm stated, we can write [5]:

$$\begin{cases} \|w_e(1 + KG)^{-1}\|_\infty < \gamma \\ \|w_e G(1 + KG)^{-1} w_d\|_\infty < \gamma \\ \|w_u K(1 + KG)^{-1}\|_\infty < \gamma \\ \|w_u KG(1 + KG)^{-1} w_d\|_\infty < \gamma \end{cases} \Leftrightarrow \begin{matrix} \|w_e S\|_\infty < \gamma \\ \|w_e G S w_d\|_\infty < \gamma \\ \|w_u K S\|_\infty < \gamma \\ \|w_u T w_d\|_\infty < \gamma \end{matrix} \quad (15)$$

5 Controller Synthesis and Robustness Analysis

Among the main components of the block diagram of the IFOC shown in Fig. 4, we find the internal current control loops for the stator currents i_{sd} and i_{sq}.

The reference current i_{sd}^* is set to a constant value, which establishes a specific magnetic state in the machine. As for the reference i_{sq}^* , it is set by the output of the speed controller.

For the synthesis of the controllers for i_{sd} and i_{sq} , we use equations (11) and (12), which describe the voltage-current model of the process. These equations are illustrated below as first-order differential equations.

$$\begin{cases} \frac{di_{sd}}{dt} = \frac{1}{\sigma L_s}\,(v_{sd1} - R_{sr} i_{sd}) \\ \frac{di_{sq}}{dt} = \frac{1}{\sigma L_s}\,(v_{sq1} - R_{sr} i_{sq}) \end{cases} \quad (16)$$

The calculations will be developed for the q-axis; the results for the d-axis are identical. σL_s and R_{sr} are uncertain. The uncertainties in these parameters can be modelled as multiplicative.

$$\begin{cases} \sigma L_s = \sigma L_{s_0}(1 + \rho_{\sigma L_s}\delta_{\sigma L_s}) \\ R_{sr} = R_{sr_0}(1 + \rho_{R_{sr}}\delta_{R_{sr}}) \end{cases} \quad (17)$$

With: $|\delta_{\sigma L_s}| \le 1$ and $|\delta_{R_{sr}}| \le 1$

The quantities $\frac{1}{\sigma L_s}$ and R_{sr} can be represented by Linear Fractional Transform (LFTs) as follows:

$$\begin{cases} \frac{1}{\sigma L_s} = F(M_{\sigma L_s}, \delta_{\sigma L_s}) \\ R_{sr} = F(M_{R_{sr}}, \delta_{R_{sr}}) \end{cases} \quad (18)$$

$$M_{\sigma L_s} = \begin{bmatrix} -\rho_{\sigma L_s} & \frac{1}{\sigma L_{s_0}} \\ -\rho_{\sigma L_s} & \frac{1}{\sigma L_{s_0}} \end{bmatrix} \; et \; M_{R_{sr}} = \begin{bmatrix} 0 & R_{sr_0} \\ \rho_{R_{sr}} & R_{sr_0} \end{bmatrix} \quad (19)$$

We then obtain the model shown in Fig. 5, represented in LFT form with uncertain parameters.

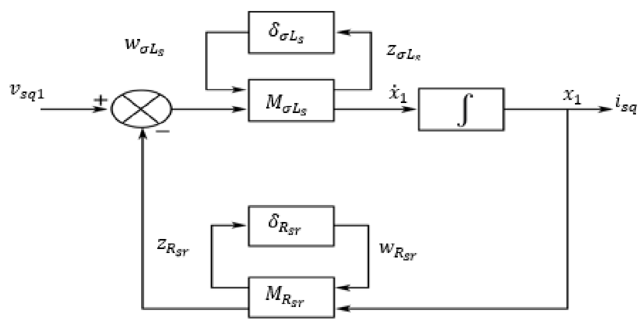

Fig. 5. Block diagram of the model with uncertain parameters.

The dynamic equations relating the inputs to the corresponding outputs, around the uncertain parameters, are rearranged as follows:

$$\begin{cases} \begin{bmatrix} \frac{di_{sq}}{dt} \\ z_{\sigma L_s} \end{bmatrix} = \begin{bmatrix} -\rho_{\sigma L_s} & 1/\sigma L_{s0} \\ -\rho_{\sigma L_s} & 1/\sigma L_{s0} \end{bmatrix} \begin{bmatrix} w_{\sigma L_s} \\ v_{sq_1} - v_{R_{sr}} \end{bmatrix} \\ \begin{bmatrix} z_{R_{sr}} \\ v_{R_{sr}} \end{bmatrix} = \begin{bmatrix} 0 & R_{sr0} \\ \rho_{R_{sr}} & R_{sr0} \end{bmatrix} \begin{bmatrix} w_{R_{sr}} \\ i_{sq} \end{bmatrix} \end{cases} \quad (20)$$

$$\begin{cases} w_{\sigma L_s} = \delta_{\sigma L_s} z_{\sigma L_s} \\ w_{\sigma L_s} = \delta_{\sigma L_s} z_{\sigma L_s} \end{cases} \tag{21}$$

If we choose the state variable x_1 and the output y as follows:$x_1 = i_{sq}$, $y = x_1$ and if we substitute the variable $v_{R_{sr}}$, into equations (20), we obtain:

$$\begin{bmatrix} \dot{x}_1 \\ z_{\sigma L_s} \\ z_{R_{sr}} \\ y \end{bmatrix} = \begin{bmatrix} -R_{sr0}/\sigma L_{s0} & -\rho_{\sigma L_s} & -\rho_{R_{sr}}/\sigma L_{s0} & 1/\sigma L_{s0} \\ -R_{sr0}/\sigma L_{s0} & -\rho_{\sigma L_s} & -\rho_{R_{sr}}/\sigma L_{s0} & 1/\sigma L_{s0} \\ -R_{sr0} & 0 & 0 & 0 \\ 1 & 0 & 0 & 0 \end{bmatrix} \begin{bmatrix} x_1 \\ w_{\sigma L_s} \\ w_{R_{sr}} \\ v_{sq1} \end{bmatrix} \tag{22}$$

$$\begin{bmatrix} w_{\sigma L_s} \\ w_{R_{sr}} \end{bmatrix} = \begin{bmatrix} \delta_{\sigma L_s} & 0 \\ 0 & \delta_{R_{sr}} \end{bmatrix} \begin{bmatrix} z_{\sigma L_s} \\ z_{R_{sr}} \end{bmatrix} \tag{23}$$

G_{sq} is the transfer matrix linking the output vector $[z_{\sigma L_s} \quad z_{R_{sr}} \quad y]^T$ to the input vector $[w_{\sigma L_s} \quad w_{R_{sr}} \quad v_{sq1}]^T$.

It represents the dynamics of the IM along the q-axis. Its state-space representation is given in Fig. 6.

Fig. 6. Input-output block diagram of the IM along the q-axis.

The input/output relationship of the uncertain system can be described by the upper LFT representation shown in the Fig.7.

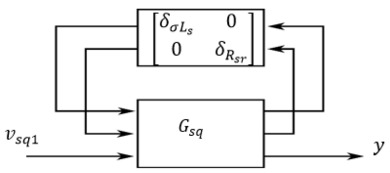

Fig. 7. The LFT representing the uncertain model of the IM along the q-axis.

6 Motor parameters

The parameters of the motor identified in the laboratory are:

$R_s = 12.75\ \Omega$; $R_r = 5.1498\ \Omega$; $L_s = 0.4991\ H$;

$L_r = 0.4331\ H$; $L_m = 0.4331\ H$;

$J = 0.0035\ Kg.m^2$; $fc = 0.001\ N.m.s.rad^{-1}$; $f = 50\ Hz$; $p = 2$.

7 Real-time implementation

The experimental platform (Fig. 9) mainly consists of the following elements: (1) Three-phase IM; (2) Three-phase voltage inverter; (3) Encoder; (4) dSpace 1104; (5) Computer, real-time monitoring and control software Control Desk; (6) Autotransformer; (7) DC power supply; (8) Currents sensors.

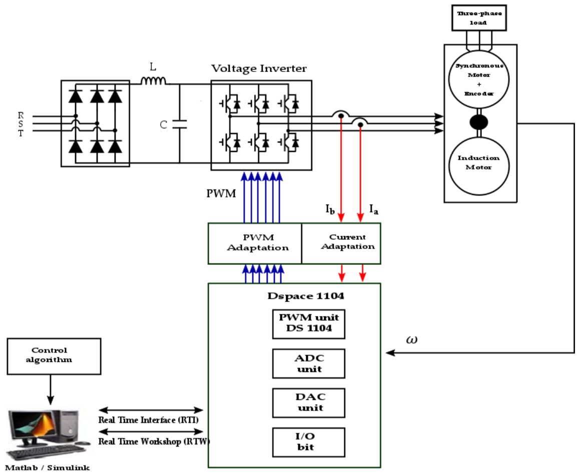

Fig. 8. Block diagram of the experimental bench.

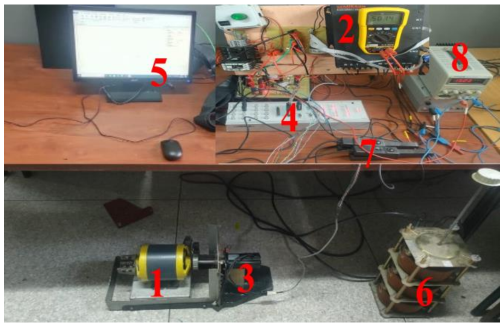

Fig. 9. Experimental bench.

8 Simulation results and discussion

Fig. 10 illustrates the simulation results of the IFOC for a step reference speed and 100% variations in stator and rotor resistances from their nominal values.

The synthesis of the robust controller is performed using MATLAB/Simulink, employing the transfer function of the current i_{sq} from equation (12) and the following weighting.

$$\begin{cases} w_e(s) = \dfrac{(10^{-3}s+10^3)}{0.5s+0.01} \\ w_u(s) = \dfrac{0.01(0.01s+0.5)}{0.1s+1} \\ w_d(s) = 0 \end{cases} \tag{24}$$

$$K(s) = \frac{1.312.10^8\, s^2 + 4.026.10^{10}\, s + 3.895.10^{11}}{s^3 + 3.637.10^5\, s^2 + 3.517.10^6\, s + 7.02.10^4} \tag{25}$$

Fig. 10 shows the step response of the transfer function of the current i_{sq} for two types of controllers: the classical PI controller and the synthesized H_∞ controller. Fig. 11, on the other hand, represents the weighting functions and their templates.

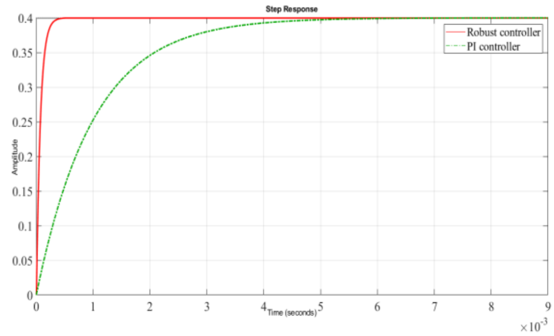

Fig. 10. System response to a step input.

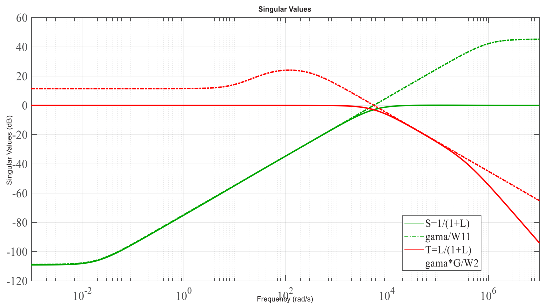

Fig. 11. Robust analysis of the system.

According to the simulation results presented in Fig. 12, we can conclude that the quality of speed control is satisfactory. Indeed, Fig. 12a shows the variation of stator and rotor resistances. Then, Fig. 12b illustrates the speed response to a reference step, while Fig. 12c presents the electromagnetic torque and the resisting torque. Fig. 12d displays the dq rotor flux, and finally, Fig. 12e highlights the dq currents along with their references.

By examining these figures, we observe a good tracking of the set point, with no significant overshoot, an absence of steady-state error, and an acceptable response time. The introduced load disturbances are quickly compensated

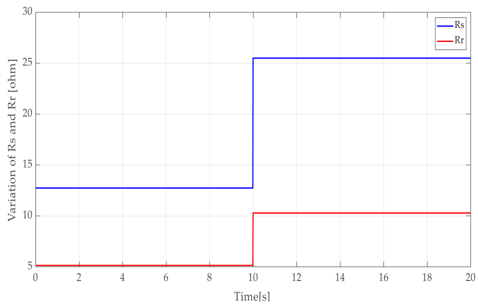

(a)

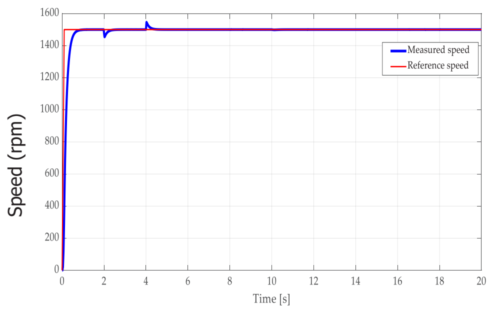

(b)

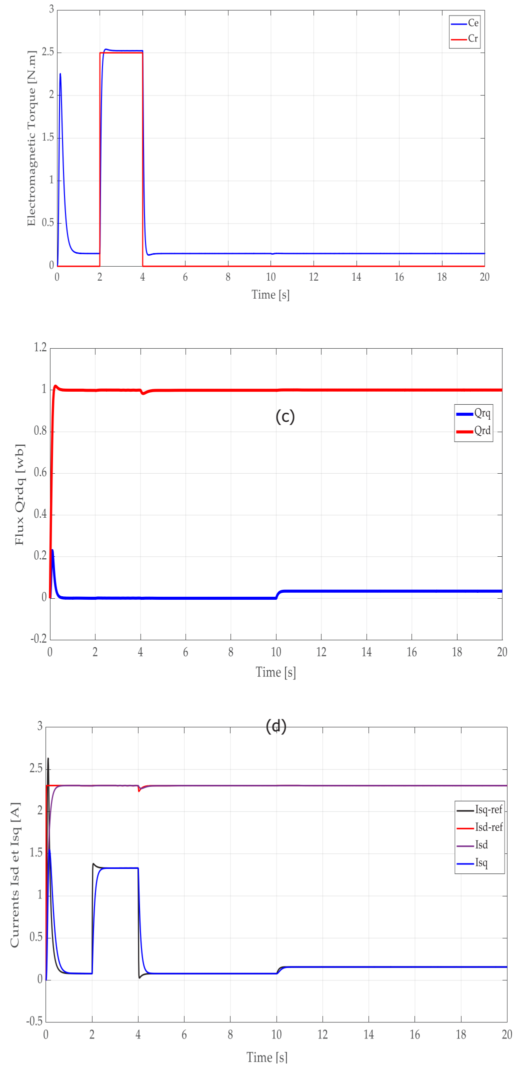

(e)

Fig. 12. Simulation results of the IFOC strategy improved by robust controllers. (a) Variations of resistances Rs and Rr, (b) Speed response, (c) Electromagnetic torque, (d) *dq* flux, (e) *dq* currents.

9 Experimental results

To validate the results of the simulation, the setup illustrated in Fig. 9 was implemented. After a start-up time of 10 seconds, resistors were added in series with the stator and rotor (wound rotor motor). This configuration allows for the modification of the resistances of the stator and rotor, thereby facilitating the evaluation of the robustness of the robust controllers.

During this experiment, we highlighted the impact of varying the rotor and stator resistances on the performance of the IFOC control system as well as its efficiency. We noted an increase in the flux level on both axes. A precise knowledge of these parameters, estimated in real-time and updated in the control, could help desensitize the IFOC strategy and enhance overall performance. It is also important to emphasize that the controllers used in this study show a significant improvement over conventional controllers.

Fig. 13a shows the variations of the resistances in the control part, while in the power part, resistors were inserted with the stator and rotor, allowing for real-time modification of the resistive parameters of the

https://doi.org/10.1051/itmconf/20246903009

asynchronous machine (IM). Subsequently, Fig. 13b illustrates the speed measurement, Fig. 13c presents a reduced portion of the current, and Figs. 13d and 13e show the flux and current profiles, respectively.

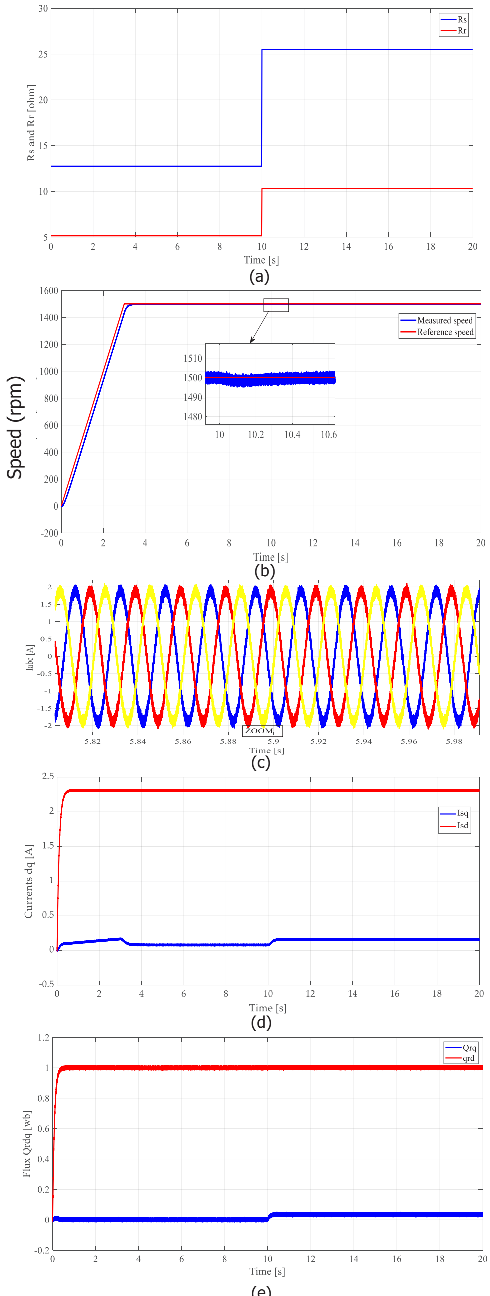

Fig. 13. Experimental results. (a) Variations of resistances Rs and Rr, (b) Speed response, (c) Currents i_{abc} (Zoom), (d) *dq* Currents, (e) *dq* Flux.

10 Conclusion

The methodology for synthesizing robust H_∞ controllers has been applied to the regulation of an induction machine. Specific controllers for current regulation were developed, and the main steps of this synthesis were detailed. The simulation results obtained for the tested machine demonstrated highly satisfactory performance, thereby proving the effectiveness of the proposed robust H_∞ technique and confirming the validity of the theoretical analysis. Furthermore, the implementation of an improved IFOCstrategy, combined with H_∞controllers, on an experimental test bench validated the simulation results. This experimental validation demonstrates the method's robustness and accuracy in practical applications, thus reinforcing its potential for industrial applications. This improvement also paves the way for further applications of robust control techniques, such as enhancing other control strategies dedicated to induction motors, like DTC and DTC-SVM.

References

1. Sowmiya, M., G. Renukadevi, and K. Rajambal. IFOC of five-phase induction motor drive. in 2013 International Conference on Power, Energy and Control (ICPEC). 2013. IEEE.
2. Lokriti, A., et al., Induction motor speed drive improvement using fuzzy IP-self-tuning controller. A real time implementation. ISA transactions, 2013. 52(3): p. 406-417.
3. Diab, A.A.Z., et al., Robust speed controller design using H_infinity theory for high-performance sensorless induction motor drives. Energies, 2019. 12(5): p. 961.
4. Rajendran, A. and S. Padma, H-infinity robust control technique for controlling the speed of switched reluctance motor. Frontiers of Electrical and Electronic Engineering, 2012. 7: p. 337-346.
5. Karimi, H.R. and H. Gao, Mixed H2/Hinfinity output-feedback control of second-order neutral systems with time-varying state and input delays. ISA transactions, 2008. 47(3): p. 311-324.
6. Boudallaa, A., et al., Real-Time Implementation of Sensorless DTC-SVM Applied to 4WDEV Using the MRAS Estimator. Energies, 2023. 16(20): p. 7090.
7. Boudallaa, A., et al., Vector control of asynchronous motor of drive train using speed controller h∞. Emerging Science Journal, 2022. 6(4): p. 834-850.
8. Boulmane, A., et al., A GA-based adaptive mechanism for sensorless vector control of induction motor drives for urban electric vehicles. Turkish Journal of Electrical Engineering and Computer Sciences, 2020. 28(3): p. 1731-1746.
9. Lee, S. and K. Lee, Current measurement offset error compensation for IFOC induction motor drives. IEEE Transactions on Industry Applications, 2023. 59(4): p. 4130-4139.
10. Kumar, P. and A.S. Hati. Sensor-less speed control of ventilation system using extended Kalman filter for high performance. in 2021 IEEE 8th Uttar Pradesh Section International Conference on Electrical, Electronics and Computer Engineering (UPCON). 2021. IEEE.